APCC
APEC CLIMATE CENTER

TECHNICAL REPORT

APCC
APEC CLIMATE CENTER

PREFACE

It is our pleasure to present to you the APEC Climate Center (APCC)'s Technical Report 2012, which reports the core outcomes of our research activities from the past year.

Since 2005, APCC, as a hub of climate information in the Asia-Pacific region, has strived to share our analysis and prediction of abnormal climate and to apply this information to regional development. The Center has established the most extensive Multi-Model Ensemble (MME) system for seasonal prediction in the world through its international science network and has provided value-added products to various stakeholders. Recently, APCC has expanded its mandate to include enhancing the capacity of APEC member economies to respond effectively to climate change and variability through better application of climate information.

In 2012, APCC continued to make an effort to improve the quality and quantity of our short-term climate forecasts and our online climate information systems, as information dissemination tools. Additionally, APCC began its endeavor to produce more applicable climate information through interdisciplinary research among various sectors, such as agriculture and hydrology. The following technical report provides more information about our research outcomes from 2012.

In 2013, following APCC's goal to enhance socioeconomic well-being through better utilization of climate information, APCC will continue to improve the quality and accuracy of its climate information, recognizing that the utility of this information is only as good as its quality. We would like to make the best use of our research outcomes in various scientific and application areas. We welcome any feedback on this report or on our services.

My best and warmest regards to all of you.

Dr. Chin-Seung Chung
Director/APEC Climate Center

CONTENTS

An Assessment of Reliability in Climate Projections of CMIP5 Models: A Cloud Variation Perspective

Dr. Sun-Hee Shin

APCC

TECHNICAL REPORT 2012-03

An Assessment of Reliability in Climate Projections of CMIP5 Models: A Cloud Variation Perspective

Dr. Sun-Hee Shin

ABSTRACT

This study examines the prediction of future changes in clouds under the effects of anthropogenic global warming, using 32 coupled models that participated in phase five of the Coupled Model Intercomparison Project (CMIP5), by comparing two runs: the historical run for 1850–2005 and the Representative Concentration Pathway (RCP) 4.5 run for 2006–2100. Metrics for evaluating the models' performance on cloud variation are designed to document performance for the period 1980–2005. The metrics include (1) the annual mean cloud; (2) the annual variation in cloud; and (3) the interannual variation in cloud. The evaluation metrics mostly consist of global and regional coefficients of spatial pattern correlation and root-mean-squared errors between the observed and the simulated results. In addition, the models' performances regarding the interannual variation in low cloud are considered through their ability to simulate the cloud meteorology correlation proposed by Clement *et al.* (2009). Based on the models' performances in simulation of the cloud variation metrics, we selected some best models for further assessment of future. Using a multi-model ensemble with the three best-performing models (B3MME) the following changes are projected in the twenty-first century under the RCP4.5 scenario: (1) The annual mean and range of cloud and cloud radiative cooling effects will decrease a significant amount, especially over the eastern north subtropical ocean, suggesting the role of positive feedback in the climate change. (2) Changes in cloud exhibit huge differences between the northern hemisphere (NH) and the Southern Hemisphere (SH). (3) There will be a more prominent temperature asymmetry between the northern and southern hemispheres due to the more evident reduction of cloud in the NH than in the SH. (4) The model spread is substantially reduced by carefully applying the evaluation metrics and selecting most reliable models. Remaining models show a good agreement in the sign and the magnitude of the cloud radiation feedback and the geographical pattern of cloud reduction in the future climate. The results of this study address the degree to which the uncertainty in global climate temperature projections can be reduced through the increased confidence in cloud feedback.

1. INTRODUCTION

It is now generally acknowledged that the climate is warming as a result of increasing greenhouse gases. However, there has been considerable uncertainty in estimating the intensity of global warming (IPCC, Meehl *et al.,* 2007). Although climate scientists and modelers in various institutes are attempting to improve the capability of global climate models and provide reliable projections of future climate change, the current models still contain huge uncertainty in the projected global warming.

How can this model uncertainty of climate change projections be reduced? One approach is to assess the reliability of key climate feedback processes, known to play a critical role in the models' estimates of climate sensitivity. In this study, we focus on evaluating cloud feedback, since clouds are one of the largest contributors to warming when levels of greenhouse gases are increased. Many previous studies have indicated and emphasized the importance of the cloud feedback process as a primary source of uncertainty in climate projections (Stephens, 2005; Bony and Dufresne, 2005; Bony *et al*., 2006; Randall *et al*., 2006; Webb *et al*., 2006; Wyant *et al*., 2006; Clement *et al*., 2009).

Clouds exert a net cooling effect on climate. In response to global warming, the cooling effect of clouds may be either enhanced or weakened, thereby exerting a cloud-radiative feedback to climate warming (Randall *et al*. 2006; NRC 2003; Zhang 2004; Stephens 2005; Bony *et al*. 2006). Klein and Hartmann (1993) showed that a one percent change in stratocumulus cloud cover (a kind of low-level cloud) could lead to a change in net Cloud Radiative Forcing (CRF) of $1Wm^{-2}$ at the top of the atmosphere, whose magnitude is roughly a quarter of the direct radiative forcing of $4Wm^{-2}$ caused by doubling atmospheric $C0_2$ concentration. A moderate change in low-level clouds can markedly offset or amplify global warming, depending on the sign of cloud feedback (Slingo 1990). Low-level clouds are the major contributor to CRF, therefore it is very important to understand how the distribution of low-level clouds will change in the future, and whether they affects the radiation balance of the Earth, either in a positive or negative way, through cloud-radiation feedback processes.

The major goal of this study is to evaluate cloud feedback in potential future climates, as predicted by current climate models. Current models are so diverse in their simulated cloud radiation feedback that approximately half of the models predict positive feedback (reduced cooling compared to the present), and the remaining half models predict negative feedback (increased cooling compared to the present; Soden and Held 2006; Webb *et al*. 2006). Several studies indicate that this model spread is mostly attributable to differences in shortwave (SW) cloud feedback, and that the responses to global warming of both deep convective clouds and low-level

clouds differ among General Circulation Models (GCMs) (Bony and Dufresne 2005; Wyant *et al*. 2006). These studies further suggest that the simulated response of low-level clouds is the major contributor affecting the degree of global warming in response to increased greenhouse gases. Bony *et al*. (2006) and Webb *et al*. (2006) examined the CRF sensitivity to sea surface temperature (SST), predicted by two groups of models in different regimes of large-scale tropical circulation. They concluded that the spread of tropical cloud feedbacks among the models arises primarily from inter-model differences in the radiative response of low-level clouds in the regime of large-scale subsidence.

Since there is no observational evidence to verify projections of future cloud feedback in a substantially warmed climate, this study suggests a methodology to validate the model simulation under the current climate conditions. It is argued that a reliable prediction of cloud feedback in future, warmer climates should be obtained by models that can reproduce a robust response of low-cloud variation in the current climate. Several studies (e.g., Klein and Hartmann 1993; Norris and Leovy 1994; Wood and Hartmann 2006) focused on the environmental controls on low-level clouds, and have shown that changes in local meteorological conditions can explain much of the low-cloud variability on daily to interannual time scales. In particular, Norris and Leovy (1994) found a negative correlation between SST and low-level cloud. Their study noted the transition from stratiform to cumuliform clouds in regions with a strong SST gradient, with stratiform clouds forming on the cooler side. Wyant *et al*. (1997) used a two-dimensional eddy-resolving model to study the equatorward transition from stratiform to cumuliform clouds. They found that rising SST acts to destabilize marine low-level clouds, eventually leading to the entrainment of dry air into the cloud deck and the replacement of stratus cloud with cumulus. Bony and Dufresne (2005) showed a breakup of marine low-level cloud in the region of subsidence, producing a strong positive feedback between shortwave cloud radiative effect and SST.

Low-level cloud may be influenced by SST by means of an altering of the lower tropospheric stability (LTS), whose variation correlates negatively with SST (Klein and Hartmann 1993; Wood and Hartmann 2006). Klein and Hartmann (1993) and

Wood and Hartmann (2006) showed that low-level cloud increases when LTS is greater. Similarly, Clement et al (2009) showed that lower LTS is accompanied by higher SST in the Northeast Pacific, leading to a reduction of the total cloud cover over the region. Therefore, previous studies provide a more or less consistent finding that a reduced LTS is driven by increased SST, which in turn causes a decrease in cloud fraction by initiating a tradeoff from stratiform to cumuliform cloud cover. Williams et al. (2006) and Stowasser and Hamilton (2006) further examined the change in CRF in response to changes in LTS, large-scale vertical velocity and the lower-tropospheric relative humidity (RH). In the evaluation of atmosphere-ocean coupled GCMs, Stowasser and Hamilton (2006) suggest that the models differ most and are least realistic in regions of subsidence, and to a lesser extent in regions of deep convection.

The understanding of large-scale environmental controls on cloud cover should help in identifying important components that control cloud feedback, and assessing which of the model estimates of cloud feedback is the most reliable. This study evaluates the low-level cloud variability produced by climate models and attempts to select the most reliable models for the estimates of cloud feedback. The study will focus on comparing the interannual variation in observed and simulated cloud amounts and top of atmosphere (TOA) radiative fluxes over the tropical ocean. The variability of low-level cloud amount in response to climate change, and its relationship to possible driving factors such as atmospheric circulation and SST changes will be addressed from local and global perspectives.

2. MODEL AND DATA

2.1 Models and experiment

Climate model output was obtained from the CMIP5 multi-model data archive (http://cmip-pcmdi.llnl.gob/cmip5/index.html). Two experiments are investigated: the historical run from 1850 to 2005, and the Representative Concentration Pathways

(RCP) 4.5 run from 2006 to 2100. The historical run was used to evaluate the degree to which the models are realistic and robust in simulating the cloud variations in recent past. The RCP 4.5 run was used to estimate cloud feedback and its uncertainties under the warming climate in the 21st century. The RCP4.5 run assumes that radiative forcing will increase and then stabilize at around 4.5 Wm^{-2} after 2100, and is chosen as the "central" scenario in CMIP5 (Taylor *et al*. 2012). In total, 32 models that participated in CMIP5 are used in this study. Table 1 lists the model names, institutions, horizontal resolution of the atmospheric component, and the number of ensemble members used for each model. To ensure equal weighting from each model, we consider only one ensemble member from each CMIP5 model to form composite CMIP5 data sets. To validate the Coupled-GCMs in their historical simulations in comparison with observations, each model run was interpolated to a common 2.5° latitude × 2.5° longitude grid. The multi-model ensemble (MME) mean was constructed with equal weights. Model climatology was obtained for the 24 years from 1980 to 2005.

Seven models (CanESM2, GFDL-ESM2M, HadGEM2-CC, HadGEM2-ES, MIROC-ESM, MPI-ESM, and NorESM1-M) in the CMIP5 are Earth System Models (ESM). They include biogeochemical components that account for the important fluxes of carbon between the ocean, atmosphere and terrestrial biosphere carbon reservoirs and may in some cases include interactive prognostic aerosol, chemistry, and dynamical vegetation components (Taylor *et al*. 2012). Therefore, the CMIP5 models may have larger response to natural forcing and aerosols than CMIP3 CGCMs (Yeh *et al*. 2012). Some of CMIP5 models perform simulations with a higher resolution or a more complete treatment of atmospheric chemistry than CMIP3 CGCMs. Detailed information on CMIP5 models and experiments can be found at http://cmip-pcmdi.llnl.gov/cmip5/experiment_design.html and related papers (e.g., Taylor *et al*. 2012).

Table 1 Description of CMIP5 models used in the study.

Index	Institution	Coupled model	AGCM resolution Lon. x Lat.	Number of ensemble members
1	Commonwealth Scientific and Industrial Research Organization and Bureau of Meteorology, Australia (CSIRO-BOM)	ACCESS1-0	1.875° × 1.25°	1

Index	Institution	Coupled model	AGCM resolution Lon. x Lat.	Number of ensemble members
2	Commonwealth Scientific and Industrial Research Organization and Bureau of Meteorology, Australia (CSIRO-BOM)	ACCESS1-3	1.875° × 1.25°	1
3	Beijing Climate Center, China Meteorological Administration (BCC)	BCC-CSM1-1	2.8125° × 2.8125°	1
4	Beijing Climate Center, China Meteorological Administration (BCC)	BCC-CSM1-1-M	1.125° × 1.125°	1
5	College of Global Change and Earth System Science, Beijing Normal University (BNU)	BNU-ESM	2.8125° × 2.8125°	1
6	Canadian Centre for Climate Modeling and Analysis (CCCma)	CanESM2	2.8125° × 2.8125°	1
7	National Center for Atmospheric Research (NCAR)	CCSM4	1.25° × 0.9375°	1
8	Centre National de Recherches Meteorologiques/Centre Europeen de Recherche et Formation Avancees en Calcul Scientifique (CNRM-CERFACS)	CNRM-CM5	1.40625° × 1.40625°	4
9	Commonwealth Scientific and Industrial Research Organization/Queensland Climate Change Centre of Excellence (CSIRO-QCCCE)	CSIRO-Mk3-6-0	1.875° × 1.875°	1
10	LASG, Institute of Atmospheric Physics, Chinese Academy of Sciences and CESS, Tsinghua University (LASG-CESS)	FGOALS-g2	2.8125° × 2.8125°	4
11	LASG, Institute of Atmospheric Physics, Chinese Academy of Sciences and CESS, Tsinghua University (LASG-CESS)	FGOALS-s2	1.667° × 2.8125°	2
12	First Institute of Oceanography, SOA, China	FIO-ESM	2.8125° × 2.8125°	1
13	Geophysical Fluid Dynamics Laboratory (GFDL)	GFDL-CM3	2.5° × 2°	1
14	Geophysical Fluid Dynamics Laboratory (GFDL)	GFDL-ESM2G	2.5° × 2°	1
15	Geophysical Fluid Dynamics Laboratory (GFDL)	GDDL-ESM2M	2.5° × 2°	1
16	NASA Goddard Institute for Space Studies (NASA GISS)	GISS-E2-H	2.5° × 2°	1
17	NASA Goddard Institute for Space Studies (NASA GISS)	GISS-E2-R	2.5° × 2°	1
18	Met Office Hadley Centre (MOHC)	HadCM3	1.875° × 1.24°	1
19	Met Office Hadley Centre (MOHC)	HadGEM2-CC	1.875° × 1.24°	3
20	Met Office Hadley Centre (MOHC)	HadGEM2-ES	1.875° × 1.24°	1
21	Institute for Numerical Mathematics (INM)	INM-CM4	2° × 1.5°	1
22	Institute Pierre-Simon Laplace (IPSL)	IPSL-CM5A-LR	3.75° × 1.875°	1
23	Institute Pierre-Simon Laplace (IPSL)	IPSL-CM5A-MR	2.5° × 1.258°	1

Index	Institution	Coupled model	AGCM resolution Lon. x Lat.	Number of ensemble members
24	Institute Pierre-Simon Laplace (IPSL)	IPSL-CM5B-LR	3.75° × 1.875°	1
25	Atmosphere and Ocean Research Institute (The University of Tokyo), National Institute for Environmental Studies, and Japan Agency for Marine-Earth Science and Technology (MIROC)	MIROC5	1.40625° × 1.40625°	1
26	Atmosphere and Ocean Research Institute (The University of Tokyo), National Institute for Environmental Studies, and Japan Agency for Marine-Earth Science and Technology (MIROC)	MIROC-ESM	2.8125° × 2.8125°	1
27	Atmosphere and Ocean Research Institute (The University of Tokyo), National Institute for Environmental Studies, and Japan Agency for Marine-Earth Science and Technology (MIROC)	MIROC-ESM-CHEM	2.8125° × 2.8125°	1
28	Max Planck Institute for Meteorology (MPI-M)	MPI-ESM-LR	1.875° × 1.875°	1
29	Max Planck Institute for Meteorology (MPI-M)	MPI-ESM-P	1.875° × 1.875°	1
30	Meteorological Research Institute (MRI)	MRI-CGCM3	1.125° × 2.25°	1
31	Norwegian Climate Centre (NCC)	NorESM1-M	2.5° × 1.875°	1
32	Norwegian Climate Centre (NCC)	NorESM1-ME	2.5° × 1.875°	1

2.2 Observation

The ISCCP data are cloud data retrieved from geostationary and polar-orbiting weather satellites. The ISCCP multi-decadal record of cloudiness exhibits a well-known global decrease in cloud amounts. This downward trend has recently been used to suggest a widespread increase in surface solar heating, and a decrease in planetary albedo, the signals for which are not adequately reproduced by current GCMs. However, this trend as observed in the ISCCP data has not been replicated in surface observations (Norris 2005), or other satellite-based cloud observations (Jacobowitz *et al*. 2003; Wylie *et al*. 2005). Campbell (2004) and Norris (2000) showed that the estimated ISCCP cloud amount may be affected by satellite-related artifacts, and the decreasing trend may not be related to physical changes in the atmosphere. Since the satellites used in ISCCP were not designed for climate monitoring, the nominal cloud record suffers from spurious variability associated with changes in instrumentation, shifts in orbit, and other problems. Moreover, the ISCCP satellite intercalibration process

was imperfect, leading to similar changes in cloud cover across the entire view area of a satellite that was inconsistent with higher-quality surface observations.

To understand the observed cloud variations, the most recently released, "adjusted" ISCCP cloud cover produced by Clement *et al*. (2009) was used, where the spurious long-term variability caused by satellite artifacts and retrieval errors were removed from the ISCPP D2 monthly-mean cloud product during 1984–2008 (Rossow and Schiffer, 1999). The ISCCP Flux Dataset was also used for the analysis of cloud radiative effect (or cloud radiative forcing), which is defined as the difference in radiative fluxes between cloudy and cloud-free conditions. Other large-scale variables used in the analysis include the sea surface temperature (SST) from the Hadley center reanalysis, and the sea-level pressure (SLP), vertical velocity, surface winds, and lower tropospheric static stability (potential temperature at 700 mb minus surface temperature) from the ERA-40 reanalysis (Uppala *et al*., 2005). All observed data were interpolated to a common 2.5° latitude × 2.5° longitude grid. As with the model data, observed climatology was obtained for the 24 years from 1984 to 2005.

3. Evaluation and selection of CMIP5 models

We evaluate the ability of the CMIP5 CGCMs to simulate clouds and their radiative effect on climate during the historical run period of 1984–2005 in terms of simple metrics that are designed to better understand the physical processes by which large-scale meteorological variables influence cloud formation. The metrics include: (1) the annual mean cloud, (2) the annual variation in cloud, and (3) interannual variation in cloud. The evaluation metrics mostly consist of global and regional coefficients of spatial pattern correlation and root-mean-squared errors between the observed and the simulated results. In addition, the models' performances on interannual variation in low-cloud are considered through their ability to simulate of the cloud-meteorology correlation proposed by Clement *et al* (2009). Based on the models' performances in simulating the cloud variation metrics, some of the best models were selected for future assessment.

3.1 Annual mean cloud

The observed characteristics of the climatological-mean cloud cover are first examined using the adjusted ISCCP data. Figure 1 displays the spatial distributions of the annual-mean total, low and high cloud covers, which are obtained from the average of 1984–2005. The total cloud cover is primarily dominant over the tropics and high-latitude oceans, including the eastern tropical Indian Ocean and the Intertropical Convergence Zone (ITCZ) near the Equator, as well as the regions of major storm tracks in the mid-latitudes. These areas contribute to coverage of about 67.2% of the globe. The increase in total cloud cover is largely accounted for by high-level cloud in the tropics and mid-latitudes, where deep convection takes place associated with the ITCZ and the extratropical storm track. In contrast, low-level cloud is most abundant in the subtropical oceans, particularly in the eastern parts. The western parts of the subtropical oceans show the smallest amount of low-level cloud cover, where small trade wind cumuli are the predominant cloud type. Low clouds appear to be predominantly oceanic; low cloud amounts average 17.5% over the land but 34% over the ocean. The global average amount of the low cloud is 25.3%. The prevailing low cloud occurs especially over the subtropical oceans, which is represented by the subtropical marine cloud, exerting a strong cooling effect on climate. The CMIP5 28CGCMs' MME generally reproduces the observed features of annual mean cloud cover, including the major tropical oceanic convergence zones and the regions of major storm track in the extra-tropical Pacific, which are constrained by the good performance of the high clouds (Fig. 1). Models have difficulty in simulating realistic low cloud cover, however. Although the MME can capture the signal of low cloud over the eastern parts of the subtropical oceans, the models tends to excessively underestimate low cloud cover overall.

To objectively evaluate the models' performances on estimating annual mean clouds, we calculate the pattern correlation coefficient (PCC) and normalized root mean square error (NRMSE) between the observation and simulation for individual CGCMs and their MME over a global region of 40S–40N, 0–360E (Fig. 3). The NRMSE is the RMSE normalized by the observed standard deviation, which is calculated with reference to the global mean. Figure 3 (left panels) shows that the CMIP5 models

can reproduce the observed high cloud cover realistically, but fail to capture the observed low cloud cover. The individual models have a PCC from 0.07 to 0.79 and NRMSE from 1.43 and 2.86 for low cloud cover and a PCC from 0.62 to 0.92 and NRMSE from 0.45 to 0.98 for high cloud cover. The wide spread of total clouds' PCC and NRMSE scores among the CMIP5 models arises primarily from inter-model differences and poor performance in simulating low cloud cover. The MME and some models, such as ACCESS1-0, ACCESS1-3, GFDL-ESM2M, HadGEM2-CC, and HadGEM2-ES, show better performance in simulating annual mean cloud covers.

Clouds have a warming effect on the Earth's surface or in the atmosphere through absorption and emission of longwave radiation, and a cooling effect through reflection of the incident shortwave radiation. Climatological features of cloud radiative forcing (CRF) associated with cloud types are analyzed in Fig. 2. The net CRF is determined by the sum of longwave cloud radiative forcing (LCRF: warming effect) and shortwave cloud radiative forcing (SCRF: cooling effect) and defined as the difference between clear conditions and all-sky conditions (Ramanathan *et al*. 1989; Hartmann *et al*. 2001; Yang *et al*. 2007). Overall, clouds exert a net cooling effect on the earth. According to the International Satellite Cloud Climatology Project (ISCCP) data, the global mean cloud radiative forcing (CRF) is negative, totaling -24 Wm^{-2} during the analysis period of 1984–2005. Spatially, clouds generate a strong cooling effect over the eastern parts of subtropical ocean where low-level clouds are prevalent, and a relatively weak cooling effect over the western Pacific and Indian Ocean. In the tropics, the SCRF and LCRF are both strong and nearly cancel one another because the high clouds over the region, where deep convection is active, exert a strong warming effect with longwave (LW) and a cooling effect through strong reflection of shortwave (SW) radiation. Conversely, CRF shows a strong net cooling effect over the eastern part of the subtropical ocean because the low clouds tend to produce a small greenhouse effect with LW and strong cooling effect through reflection of SW radiation. The models' MME well captures the warming effect of LCRF, but it fails to capture the cooling effect of SCRF over the eastern subtropical oceans because of the models' shortcomings in simulating low clouds.

Fig. 3 (right panels) shows the PCC and NRMSE between observed and simulated

cloud radiative forcing, indicating that the MME is evidently better than individual models in simulating the CRF. The individual models have a PCC from 0.22 to 0.81 and NRMSE from 0.70 to 1.40 for SCRF, a PCC from 0.62 to 0.90 and NRMSE from 0.44 to 1.07 for LCRF, and a PCC from -0.12 to 0.79 and the NRMSE from 0.68 to 1.65 for CRF. The wide spread of cloud radiative forcings' PCC and NRMSE scores among the individual models is mainly due to inter-model differences in simulating SCRF through the models' inaccuracies of low cloud simulation. The MME and some models, such as ACCESS1-0, ACCESS1-3, GFDL-ESM2M, HadGEM2-CC, and HadGEM2-ES, show better performance in simulating annual mean cloud radiative forcing.

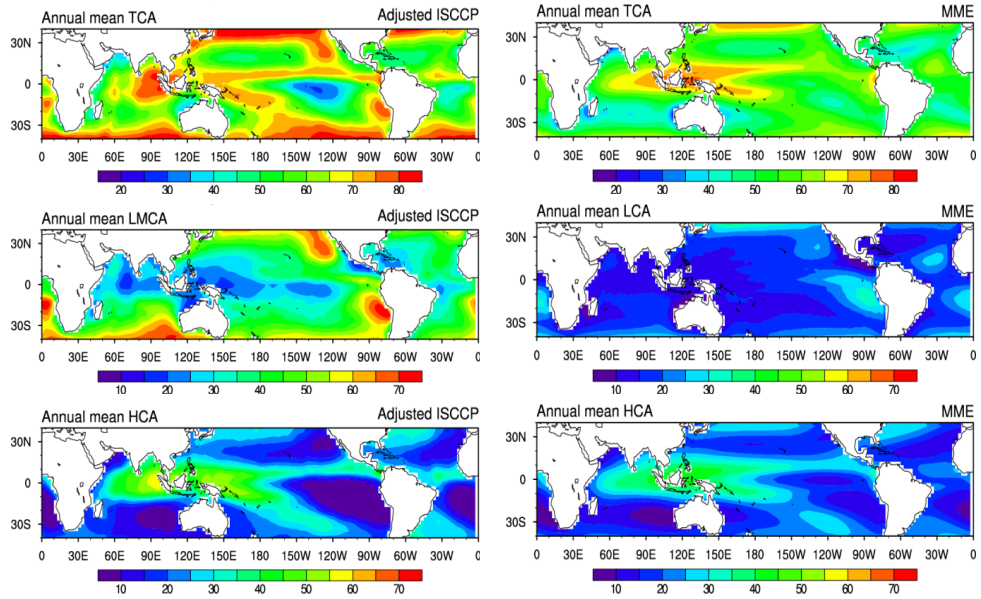

Figure 1 Comparison of cloud climatology (1984–2005) between observations (ISCCP) and 28 CGCMs' multi-model ensemble (MME): total cloud amount (TCA, %), low cloud amount (LCA, %), high cloud amount (HCA, %).

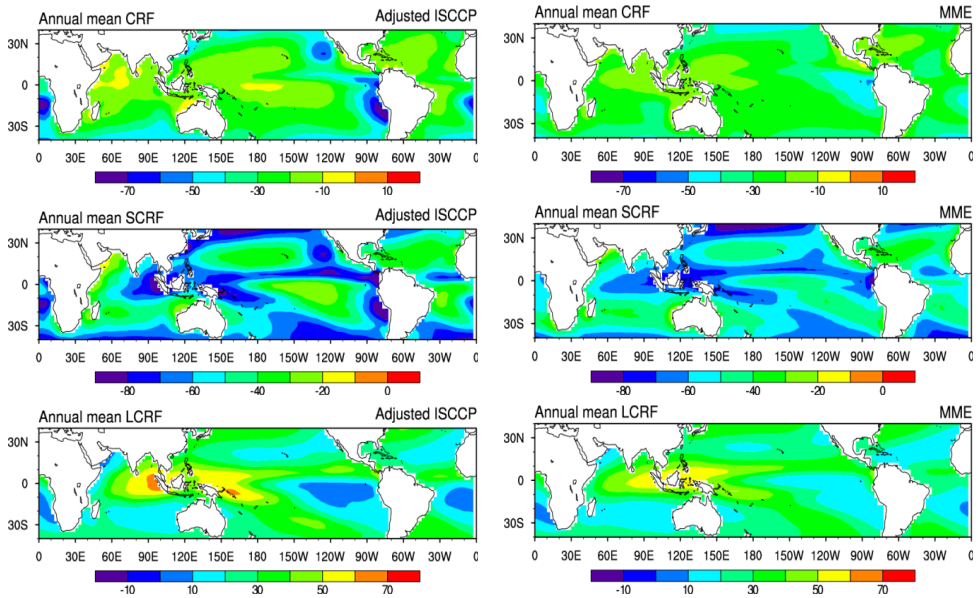

Figure 2 Comparison of cloud radiative forcing (CRF) climatology (1984–2005) between observations (ISCCP) and 28 CGCMs' multi-model ensemble (MME): net cloud radiative forcing (CRF, Wm^{-2}), shortwave cloud radiative forcing (SCRF, Wm^{-2}), longwave cloud radiative forcing (LCRF, W^{-2}).

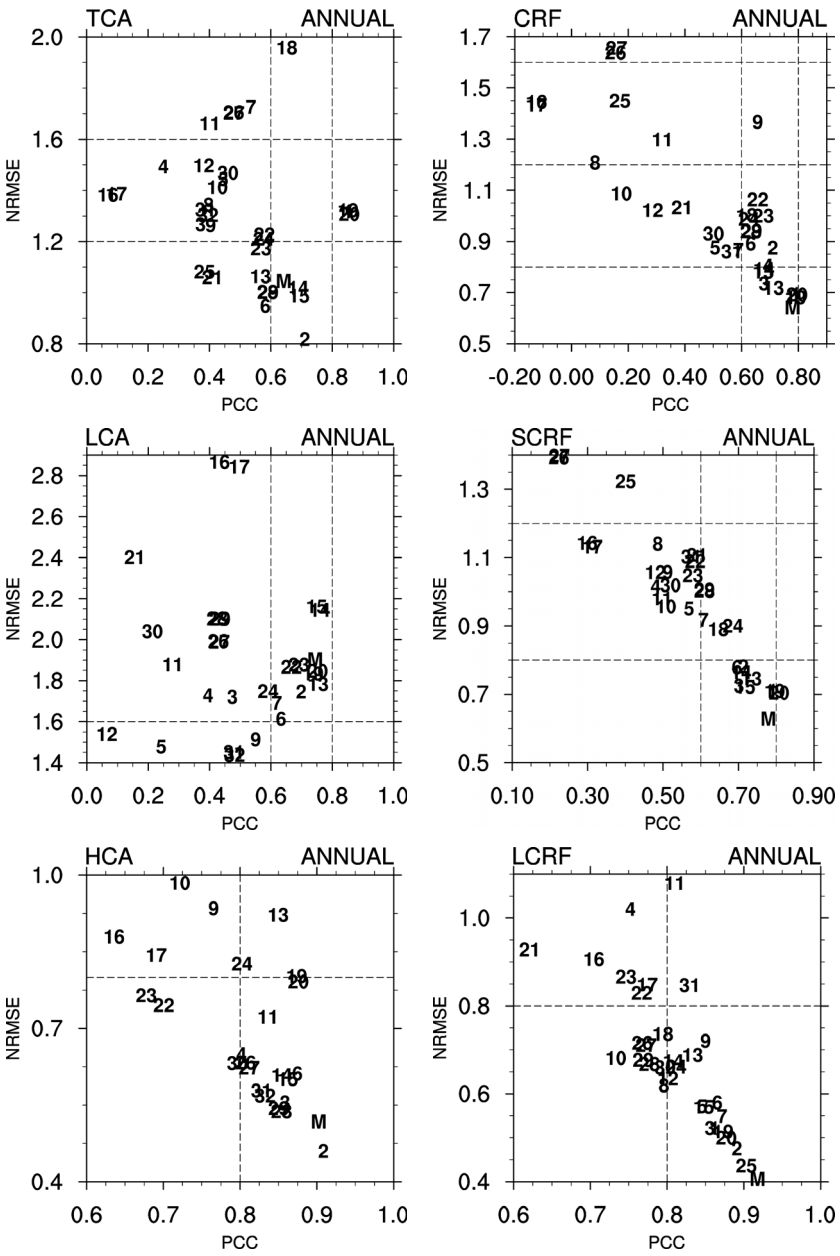

Figure 3 Performance of CGCMs and their MME on clouds and CRF climatology (1984–2005): total cloud amount (TCA, %), low cloud amount (LCA, %), high cloud amount (HCA, %), net cloud radiative forcing (CRF, Wm^{-2}), shortwave cloud radiative forcing (SCRF, Wm^{-2}), longwave cloud radiative forcing (LCRF, Wm^{-2}). The abscissa and ordinates are pattern correlation coefficient (PCC), and domain-averaged RMSE normalized by the observed spatial standard deviation (NRMSE), respectively. The domain used is 40°S-40°N, 0°-360°E.

3.2 Seasonal variation in cloud amount

In order to assess the degree of annual variation, the standard deviations of monthly means in clouds and cloud radiative forcings are computed from the following equation:

$$\mathrm{SSD} = \sqrt{\frac{\sum_{n=1}^{N}(x_n - \bar{x})^2}{N-1}}$$

where SSD denotes the seasonal standard deviation, N is 12 (months), x represents the monthly mean fields of cloud amount, while $\bar{x}$ is the annual mean field of the cloud amount.

Seasonal variations in SSD are evident and reflect the dominant seasonal temporal features of clouds. Fig. 4 and Fig. 5 display the spatial distributions of the annual amplitude and phase of total, low and high cloud covers. Strong annual variations in total cloud are found over tropical oceans such as the western coast of Central America, the Indian monsoon region, and the southern ocean of Indonesia, where deep convective clouds are prominent. High cloud cover changes seasonally, including southward and northward shifts in January and July, respectively. This pattern includes shifts over Africa, the southeast Asia/Maritime Continent monsoon complex, and South America. Seasonal shifts in these regions are closely related to the seasonal migration of monsoon-like activity. Annual variation in the total cloud is also evident over the western coastal region of America and Africa, connected to the seasonal cycling of low cloud. During January, low-level clouds show obvious maxima in the southeastern China Sea, the Circumpolar Ocean, and the storm track regions of the North Pacific and the North Atlantic. In addition, low clouds are seen in the marine subtropical north-eastern oceans near the Californian and Canarian coasts during July, and Peruvian and Namibian regions during September, where sea surface temperature is comparatively low and where the mean air motion is downward. The annual variations in total cloud well reflect both cloud seasonalities. The CMIP5 28CGCMs' MME generally reproduces the observed features of cloud seasonality, especially the seasonal cycle of high clouds. However, models have difficulty in simulating realistic annual variation in low cloud cover. Although the MME can capture

the signal of low cloud variation over the eastern parts of the subtropical oceans, the models tends to excessively underestimate the intensity of low cloud variability overall. Fig. 7 shows the PCC and NRMSE between observed and simulated annual amplitude of clouds. The MME shows better performance than individual models in simulating the annual intensity of cloud variation. The individual models have a PCC from 0.29 to 0.70 and NRMSE from 0.76 to 1.61 for TCA, a PCC from 0.13 to 0.58 and NRMSE from 0.94 to 1.82 for LCA, and a PCC from 0.01 to 0.83 and NRMSE from 0.64 to 1.63 for HCA. The MME and some models, such as ACCESS1-0, GFDL-ESM2G, GFDL-ESM2M, HadGEM2-CC, and HadGEM2-ES, show better performance in simulating annual variation in clouds.

Annual variations in CRF (Fig. 6) are influenced by cloud variability in a variety of ways. In the tropics, the LCRF and SCRF nearly cancel one another over many areas. This is expected over areas such as the central Pacific, western Atlantic, and the Arabian Sea, where little cloudiness is seen. Strong annual amplitude of cloud forcing variation is found over the storm tracks at middle latitudes in the winter hemisphere, where the cloud albedo effects outweigh the greenhouse effects. The most extreme values occur over eastern subtropical marine areas. The CMIP5 MME captures the seasonality of CRF reasonably well, although it simulates a weak intensity of annual variation in CRF over the subtropical marine areas where the low cloud is dominant. As shown in Fig. 7, the MME is evidently better than individual models in simulating the annual intensity of cloud radiative forcing. The individual models have a PCC from 0.36 to 0.77 and NRMSE from 0.68 to 1.19 for SCRF, a PCC from 0.51 to 0.84 and NRMSE from 0.54 to 1.53 for LCRF, and a PCC from 0.48 to 0.88 and the NRMSE from 0.60 to 1.09 for CRF. The MME and some models, such as ACCESS1-0, HadGEM2-CC, and HadGEM2-ES, show better performance in simulating annual variation in cloud radiative forcing.

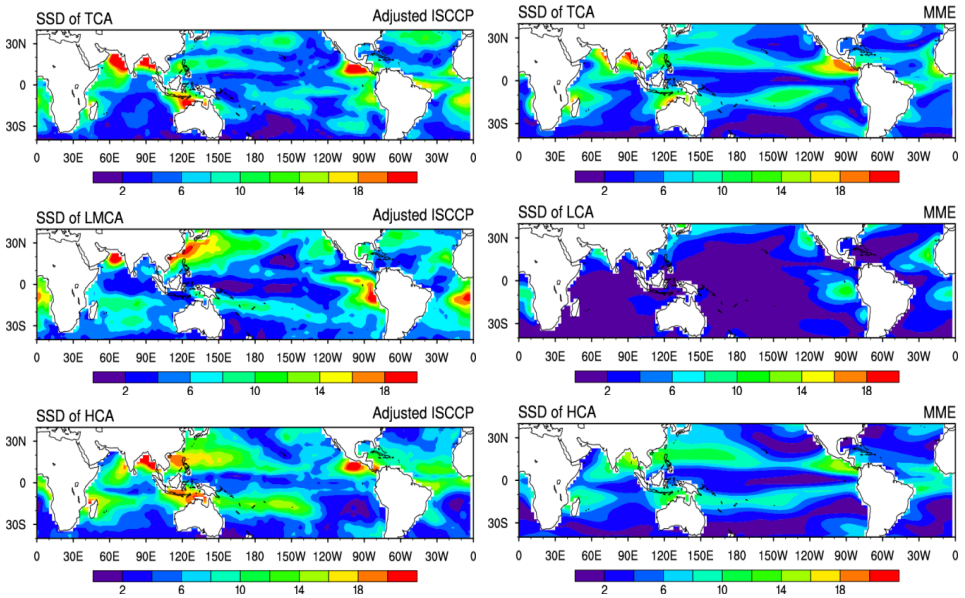

Figure 4 Comparison of annual amplitude of clouds (1984–2005) between observations (ISCCP), and 28 CGCMs' multi-model ensemble (MME): total cloud amount (TCA, %), low cloud amount (LCA, %), high cloud amount (HCA, %).

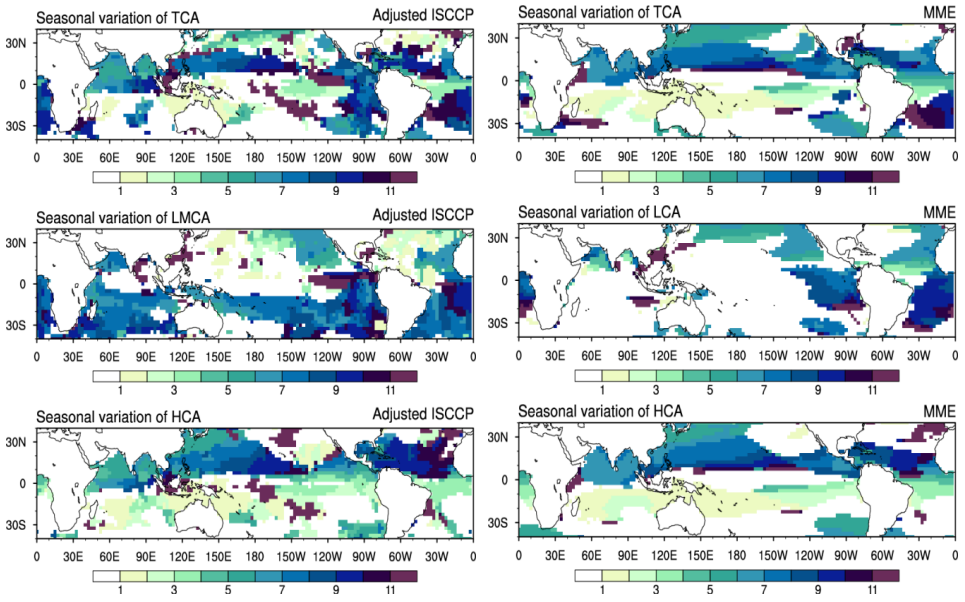

Figure 5 As for Figure 4, but showing annual maximum phase of clouds.

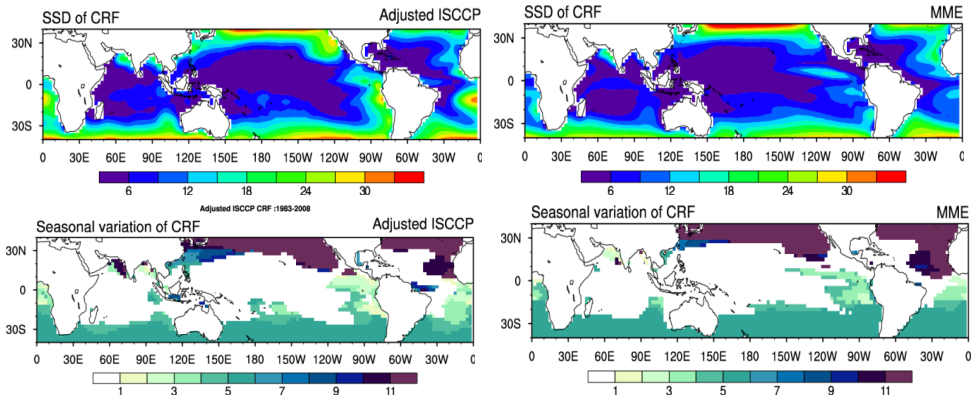

Figure 6 Comparison of annual amplitude and maximum phase of net cloud radiative forcing (CRF) (1984–2005) between observations (ISCCP) and 28 CGCMs' multi-model ensemble (MME).

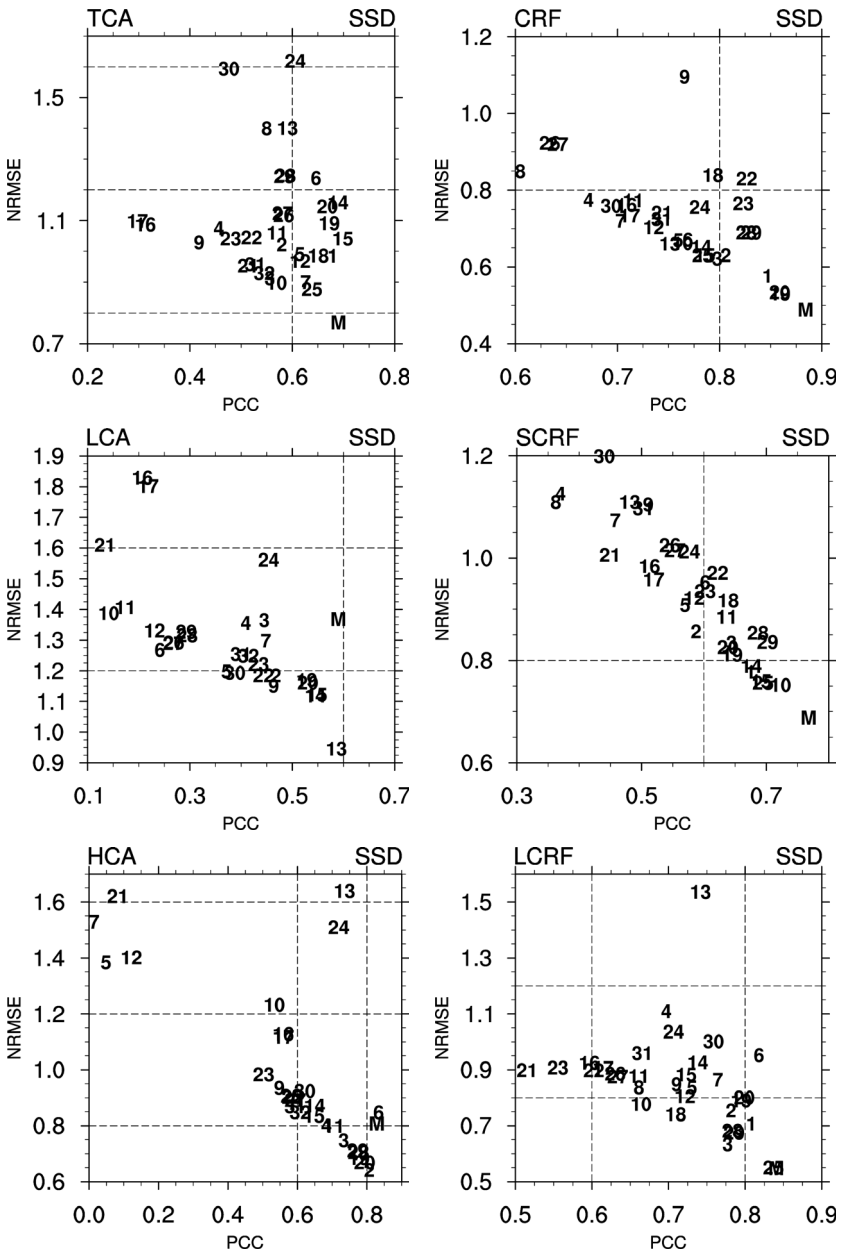

Figure 7 Performance of CGCMs and their MME on the seasonal standard deviation (SSD) of total cloud amount (TCA, %), low cloud amount (LCA, %), high cloud amount (HCA, %), net cloud radiative forcing (CRF, Wm^{-2}), shortwave cloud radiative forcing (SCRF, Wm^{-2}), longwave cloud radiative forcing (LCRF, Wm^{-2}). The abscissa and ordinates are pattern correlation coefficient (PCC) and domain-averaged NRMSE, respectively. The domain used is 40°S-40°N, 0°-360°E.

3.3 Interannual variation in cloud amount

Clement *et al*. (2009) proposed a method to test the realism of the cloud simulation in current-generation climate models through the cloud-meteorology correlation test. In this study they suggested that a larger number of climate models should be considered with regard to the relationships between cloud cover and regional meteorological conditions, to ensure greater confidence in the sign of the low cloud feedback response to future changes in greenhouse gas concentrations. To validate the CMIP5 models' simulation of inter-annual cloud variations, temporal correlations between cloud cover and large-scale meteorological variables such as SST, lower tropospheric stability (LTS), and sea level pressure (SLP), are computed. The correlations are calculated using the monthly-mean anomalies relative to long-term monthly means. A total of 264 months (12 months over 22 years) have been used for correlation, whose coefficient greater than 0.2 is statistically significant at the 99% level. Using the observed cloud-meteorology correlation, the model performance in cloud inter-annual variations is assessed according to the sign of the correlation relative to observations and comparison of their spatial pattern. The seasonal cycle is removed from the monthly means by subtracting long-term monthly means.

Fig. 8 shows the correlation between the SST and cloud cover, which is separated into total, low, and high clouds. Correlation patterns differ depending on the cloud types. Over wide regions, low clouds are negatively correlated with SST, except for a weak positive correlation in the off-equatorial region of the central Pacific. Negative correlations are particularly strong over the eastern parts of the subtropical ocean and along the Equator in the Pacific. Such a correlation is consistent with previous observational studies (Clement *et al*.; 2009; Eastman *et al* 2011; Norris and Leovy 1994; Wyant *et al*. 1997). On the other hand, high clouds show a positive correlation with SST in the equatorial Pacific, but elsewhere show little correlation. The correlation pattern of total cloud amount indicates the negative correlation over eastern parts of the subtropics with persistent low cloud, and the positive correlation in the equatorial Pacific associated with strong convection activity, thus a superposition of the two: low and high cloud correlation patterns. The 28 models' MME well reproduces the high cloud response to the SST in the equatorial Pacific, but cannot

simulate the low cloud response to SST, especially in eastern parts of subtropical oceans, because of the underestimated low cloud in that region. The individual models (not shown) generally show worse performance in the simulation of low cloud response to the SST than the MME. However some models, most markedly ACCESS1-0, CCSM4, HadGEM2-CC, HadGEM2-ES, IPSL-CM5B-LR, and NorESM1-ME, well reproduce the low cloud response to the SST. The strength and spatial extent of the high and low cloud response to SST are well represented compared with observations, with maximum positive correlations of 0.6–0.8 in the equatorial central Pacific (high cloud response) and negative correlations of 0.2–0.4 over the subtropical marine area (low cloud response).

According to the Klein and Hartmann (1993), the low cloud variation is more closely correlated to the stability variation rather than that of the SST. Fig. 9 shows the relationship between LTS and total, and low cloud covers. While the low cloud shows a negative correlation with SST, it consistently has the strongest relationship with variations in LTS. A reduced LTS can be caused by increasing SST, which causes a decrease in cloud fraction by initiating a tradeoff from low clouds to high clouds (Wyant *et al.* 1997). As expected, high cloud shows the opposite correlation compared to the low cloud (not shown). As a result, the correlation pattern of total cloud amount shows a positive correlation with LTS in the regions of persistent marine low cloud and a negative correlation in the equatorial Pacific. The models' MME can capture the observed spatial pattern of cloud response to LTS, including the negative correlation of high cloud in the equatorial central Pacific and the eastern India Ocean, and positive correlation of low cloud over eastern subtropical oceans, although it reveals a positive correlation (incorrect sign compared to observations) in the equatorial eastern ocean. A few individual models, ACCESS1-0, CCSM4, GFDL-ESM2M, HadGEM2-CC, and HadGEM2-ES, (not shown) also well represent the strength and spatial extent of the observed spatial pattern, with maximum negative correlations in the equatorial central Pacific and positive correlations over subtropical marine areas.

Besides SST and LTS, which are supposed to control the atmospheric thermal structure, other factors like large-scale circulation may also play an important role in the variation in low clouds. George and Wood (2010) suggest that changing SLP,

associated with changing circulation, plays a role in modulating low cloud. Fig. 10 indicates the correlation of cloud cover with the local SLP, which should give a measure of the strength of subsidence. The observed total cloud amount correlated with SLP shows a negative correlation throughout the tropical and subtropical ocean, with maximum of around 0.6 in the western Pacific Ocean, while it reveals significant positive correlations over the subtropical eastern marine areas. Although the MME reproduce the high cloud response over western pacific and Indian Ocean

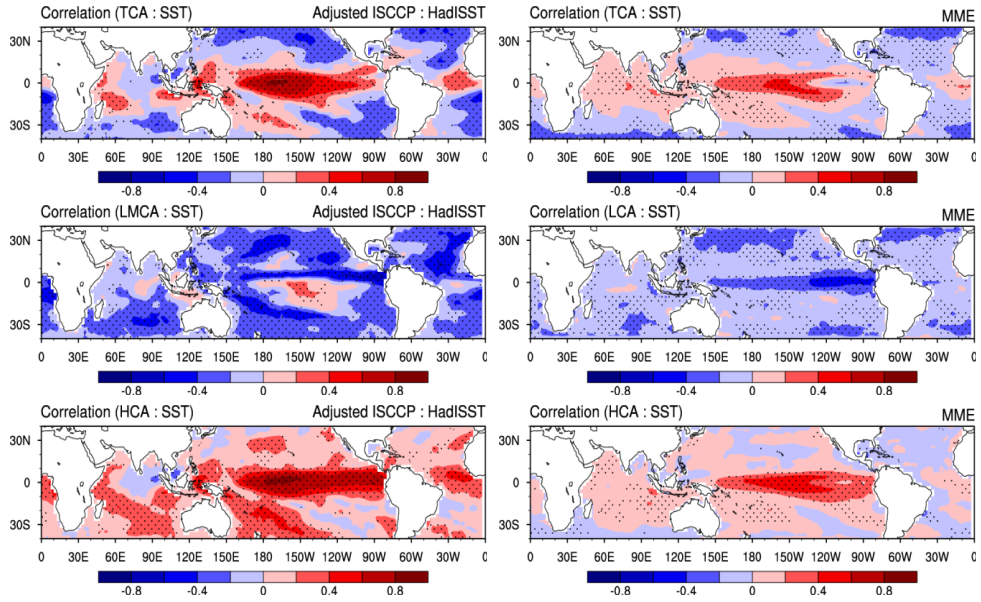

Figure 8 Correlation between SST (UK Met Office HadISST1) and (upper) total cloud cover, (middle) low cloud cover, and (bottom) high cloud cover: (left panels) observation (ISCCP) and (right panels) 28 CGCMs' multi-model ensemble (MME). Correlations are shown as shaded colors: red colors represent positive correlations and blue colors represent negative correlations. Cloud amount and SST anomalies are monthly anomalies relative to long-term monthly means. Stippling indicates significance at the 99% level.

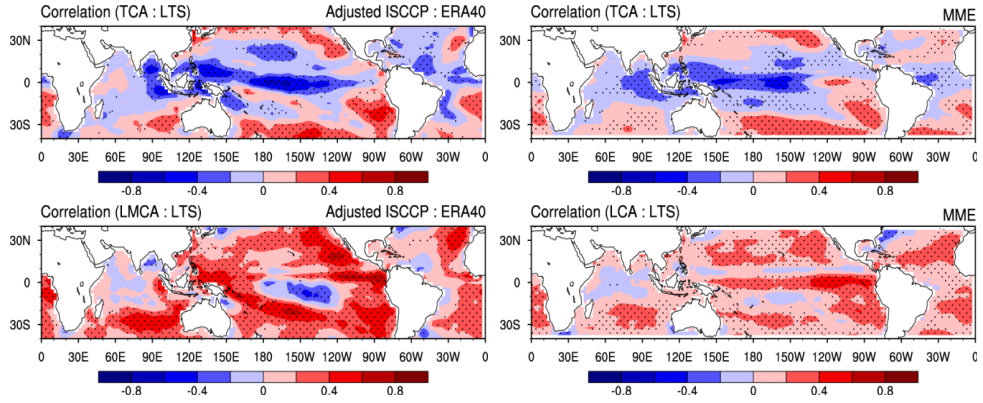

Figure 9 Correlation between LTS and (upper) total cloud cover, and (bottom) low cloud cover: (left panels) observation and (right panels) 28 CGCMs' multi-model ensemble (MME).

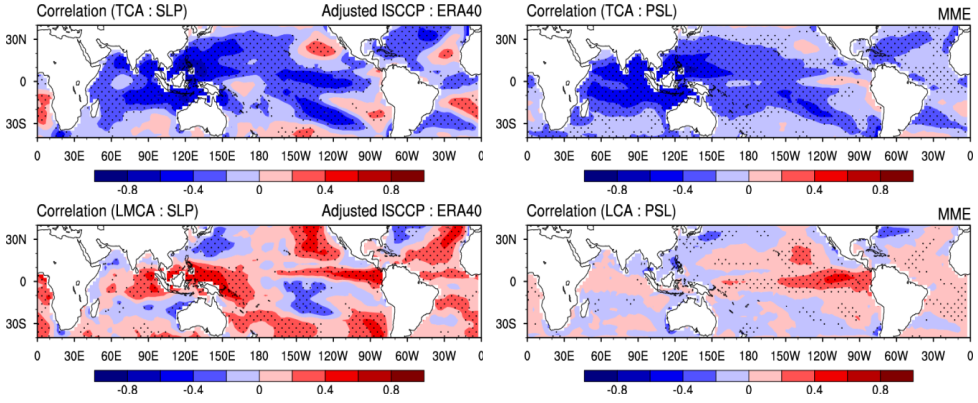

Figure 10 As for Figure 9 but showing correlation with sea level pressure.

fairly well, it is less realistic in capturing the positive correlation of the low cloud over the eastern subtropical ocean. In the case of models CCSM4 and GFDL-ESM2M (not shown), the positive correlations over subtropical eastern ocean are fairly well matched to the observations, but the negative correlations in the western Pacific are overly weak or extensively extended to higher latitudes. The Access1-0, HadGEM2-CC and the HadGEM2-ES also well represent the overall structure of cloud response to SLP, however they tend to overly reproduce the positive correlation in the subtropical and equatorial eastern Pacific. In our examination, other variables such

as RH and surface wind speed show little correlation with clouds.

As illustrated in Fig. 8 to Fig. 10, the correlation patterns of total cloud cover show the well-combined structure of low and high cloud correlation patterns, reflecting the negative correlation over eastern parts of subtropics with persistent low cloud and the positive correlation in the equatorial Pacific with strong convective activity. In Fig. 11, we summarize the veracity of model simulations in reproducing the observed relationship between the total cloud cover and the large-scale variables, by comparing the pattern correlation coefficients between the observed and the modeled spatial correlation patterns. Coefficients are based on the oceanic domain between 40° S and 40° N, and 0° E to 360° E. While most models poorly reproduce the spatial pattern of the cloud response to the change in meteorological variables, the MME and seven models show pattern correlation coefficients over 0.6 for all variables; these models are ACCESS1.0, CCSM4, GFDL-ESM2M, HadGEM2-ES, HadGEM2-CC, NorESM1-M and NorESM1-ME. Note that it is possible to obtain a perfect correlation without reproducing the correct magnitude at all. This means that a model which is only weakly sensitive (or oversensitive) to meteorology can appear perfectly correlated with observations, just because it can reproduce the spatial pattern of positive and negative. Therefore, we cautiously examine the individual models' spatial patterns of correlation between total cloud and meteorological variables (not shown). Among the six selected models, some (ACCESS1.0, HadGEM2-ES and HadGEM2-CC) reproduce the observed spatial pattern of cloud response to the changes in all variables quite well, including the contrasting responses over the tropical Pacific and subtropical eastern oceans, as well as their strength. Although the CCSM3, GFDL-ESM2M, NorESM1-M and NorESM1-ME models have similar values of pattern correlation for all variables, they are unable to reproduce the low cloud response over the eastern subtropical oceans, so they fail to capture the contrasting structure of cloud response to the change of meteorological variables.

Low clouds are the major contributor to CRF and contribute significantly to the net cooling effect on the climate. Therefore focus is placed specifically on the model simulations over the low cloud prevailing regions defined in Table 2. In Fig. 12, we compare the domain-averaged correlation coefficients between the total cloud

cover (in this case, mostly low-level cloud) and SST, LTS, and SLP, respectively, for each model and the observation. As no models in this study are able to provide the cloud fraction to retrieve low cloud, we use the total cloud cover, instead, for the evaluation of CGCMs ability to simulate the low cloud response to the meteorological variables. This is a reasonable substitution, particularly in the subtropical marine areas where the total cloud cover is mostly made up of low clouds and well reflects the low cloud properties. We also used low-level cloud results from 28 models that do provide the cloud fraction, which produced similar results. Over the defined regions, the observed correlations of cloud cover show a negative sign for SST and positive signs for LTS and SLP, consistent with the previous discussion. Models are selected according to whether they have the correct sign correlation relative to observations. On this basis, only three models are selected, ACCESS1.0, HadGEM2-ES, and HadGEM2-CC, which simulate the correct sign correlations for all three investigated large-scale variables.

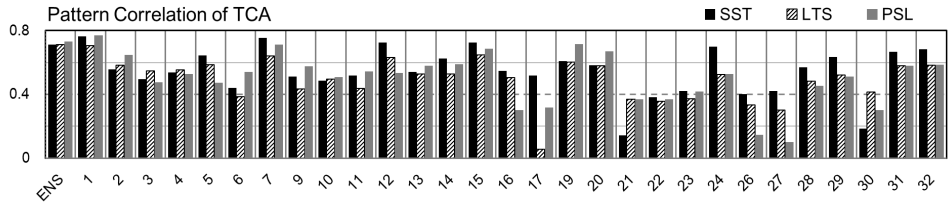

Figure 11 Pattern correlation coefficients of correlation between total cloud amount and various meteorological quantities for observations and climate models. Each coefficient is averaged over the ocean with 40S–40N in latitude and 0–360 in longitude. Each number corresponds to a particular GCM (see Table 1).

Table 2 The four low cloud regions and their geographical extent.

	Region	Location
1	Peruvian	10S–20S, 80W–90W
2	Namibian	10S–20S, 0E–10E
3	Californian	20N–30N, 120W–130W
4	Canarian	15–25N, 25–35W

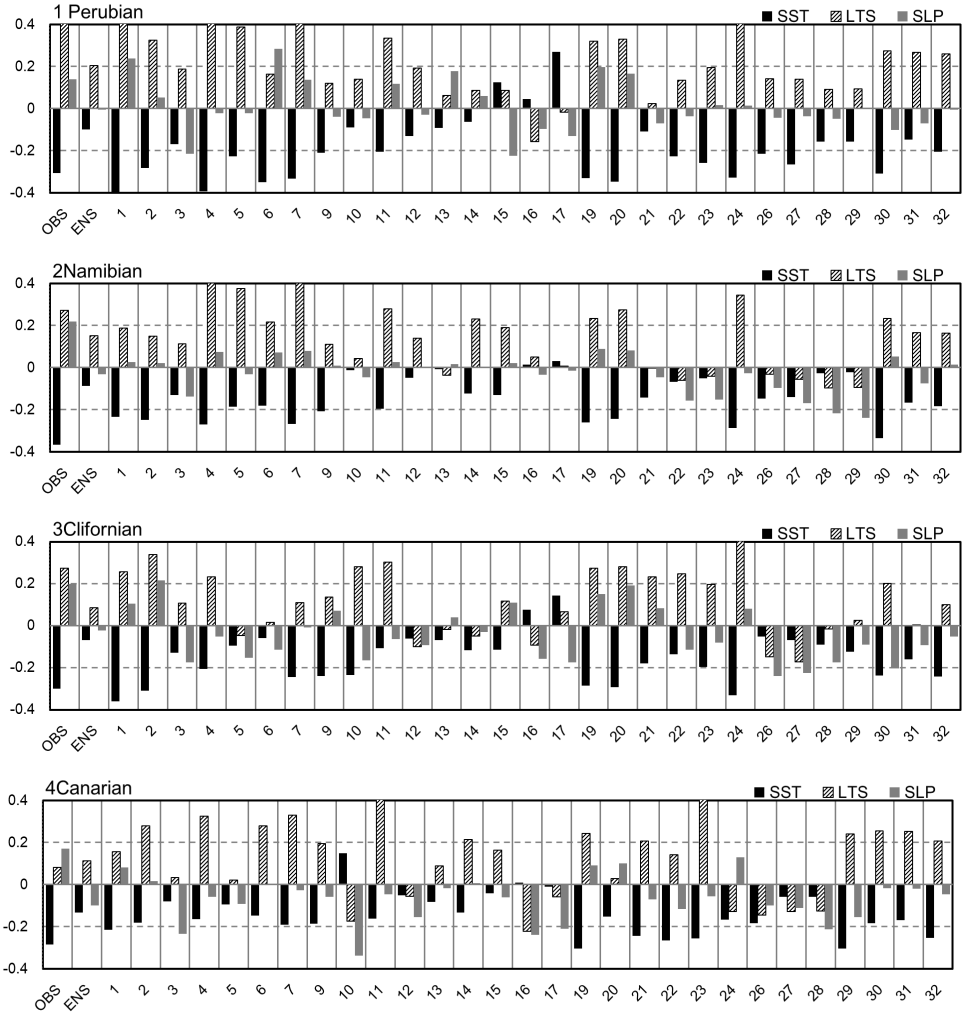

Figure 12 Correlation between total cloud cover and various meteorological quantities in four marine areas for observations and climate models. Each number corresponds to a particular AOGCM (see Table 1). The selected areas are indicated Table 2, defined by Klein and Hartmann (1993). For the comparison, the total cloud amounts are correlation with observed SST (black bar), lower tropospheric stability (LTS, slashed bar) and sea level pressure (SLP, gray bar).

3.4 Best model selection

Based on the PCC and NRMSE for the annual mean cloud and seasonal variation, and cloud-meteorology correlation test for the interannual variation in cloud, the three best models are selected, whose MME has a better skill with much less uncertainty than the 32 model's MME, especially in capturing the low level cloud variations and CRF (not shown). The three best models are ACCESS1-0, HadGEM-CC and HadGEM-ES. These three selected models show the best performance not only in the cloud-meteorological variations but also in the mean and seasonal variation in cloud cover and CRF. The observed net radiative forcing represents an average net cooling effect of -21.4 Wm^{-2} at the top of the atmosphere, with longwave warming of 27.4 Wm^{-2} and shortwave cooling of -52.2 Wm^{-2}. The total cloud cover is observed to be around 62.4%. The three best model's MME (B3MME, hereafter) exhibits considerably good agreement with the observations in terms of the magnitude of the net cloud radiative forcing, as well as the individual shortwave and longwave components. The B3MME also represents the smallest root mean square error (RMSE) and the highest pattern correlation coefficient of annual mean and seasonal standard deviation in cloud and CRF.

4. Future changes in cloud radiative forcing by global warming

In this section, we discuss future changes in clouds and their impact on the climate, by comparing climatological means during the historical run period (1950–1999) with the RCP4.5 run period (2050–2099) using the CMIP5 B3MME selected in Sect. 3. The primary goal is to understand how the cloud radiative feedback would operate in a future global warming circumstance, because the current GCMs are diverse in their results when simulating the cloud radiative feedback, even regarding the sign of change.

Fig. 13 shows the mean cloud changes and their impact on climate, as simulated by B3MME and the 21 models' MME. In Fig. 13, stippling indicates area where the

magnitude of the change of the MME exceeds the uncertainty, as measured by the standard deviation of inter-model spread against the MME. The CMIP5 B3MME projects a significant decrease in total cloud cover over most parts of the subtropical oceanic region, especially over the northern hemisphere oceanic regions, and an increase over the equatorial Pacific, equatorial Atlantic Ocean and Eastern South Pacific. In addition, the changes are more prominent over the eastern subtropical ocean than the western parts, which is mainly due to the changes in low cloud cover. The changes in the cloud cover correspond well to changes in the cloud radiative forcing. Reduced cloud cover occurs off the west coast of North America with the local maximum in SST change. Conversely, increased cloud cover is seen off the west coast of South America, accompanying a minimum in SST change. Spatial patterns of change in the cloud cover and the cloud-radiative forcing seem to be well explained by the SST change. Considering that low clouds dominate shortwave cooling, while high clouds dominate longwave warming, the evident increase in SST warming may be induced by large reduction of low cloud cover off the west coast of North America and the eastern equatorial Pacific, contributing to positive CRF changes. The increased total cloud cover in the equatorial Pacific can be understood as an increase in the amount of high cloud or a tradeoff from low clouds to high clouds. The spatial distribution of the projected changes by the 21 models' MME is very similar to that by the B3MME, although the amplitude of the change is smaller and its uncertainty (inter model spread) is much larger in the former.

We evaluate the cloud-radiative feedback (i.e., the CRF change) in future climates using the best three selected models. Fig. 14 shows the changes in the cloud radiative forcing for the three individual models. The CRF change is divided by the magnitude of the SST increase in each model. The best three models exhibit quite good agreement in their projected cloud forcing changes, with negative signs in the longwave radiation and positive signs in the shortwave radiation. Overall, the models exhibit radiative warming induced by cloud changes, although the magnitude is somewhat larger in the HadGEM2-ES model. The decrease in the total cloud cover is mainly caused by the reduction of low cloud cover. It is important to note that B3MME predicts positive feedback (less cooling than the present) in future climate, which is mainly caused by the reduced shortwave cooling effect caused by low cloud reduction.

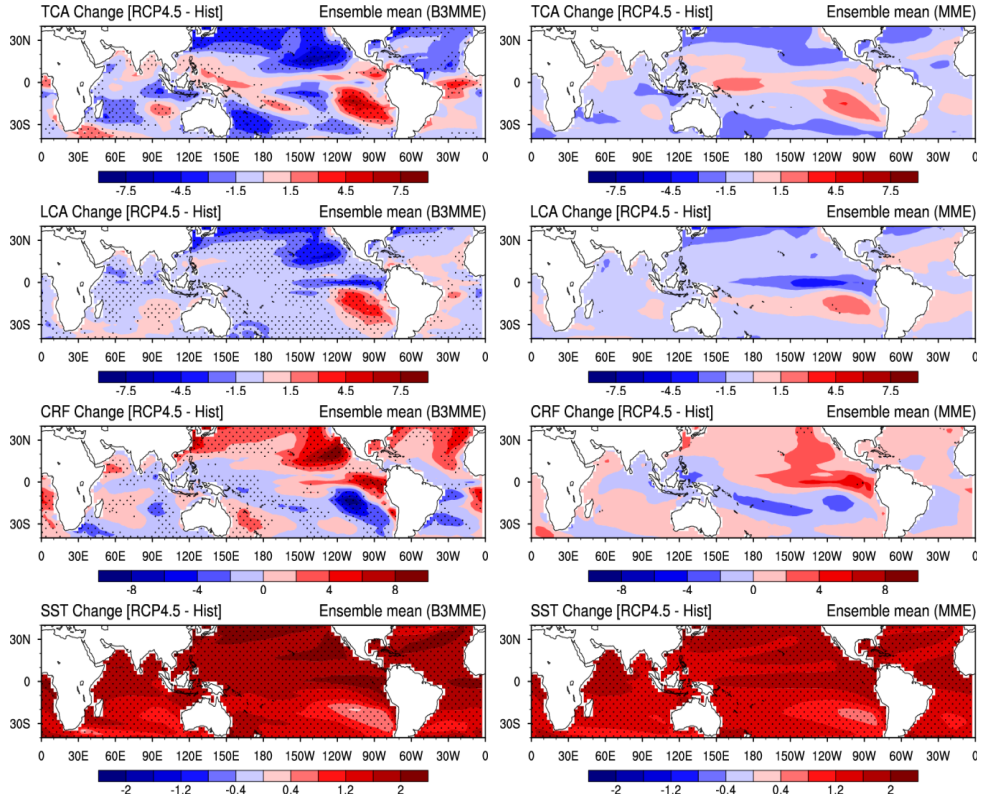

Figure 13 Changes in total cloud cover (TCA), low cloud cover (LCA), cloud radiative forcing (CRF) and sea surface temperature (SST) for the best three models' (B3MME) and 21 models' MME (MME). Changes are given for the RCP4.5 simulation for the period 2050–2099 relative to the historical simulation for the period 1950–1999 in CMIP5. Stippling denotes areas where the magnitude of the ensemble mean exceeds the standard deviation of inter-model spread.

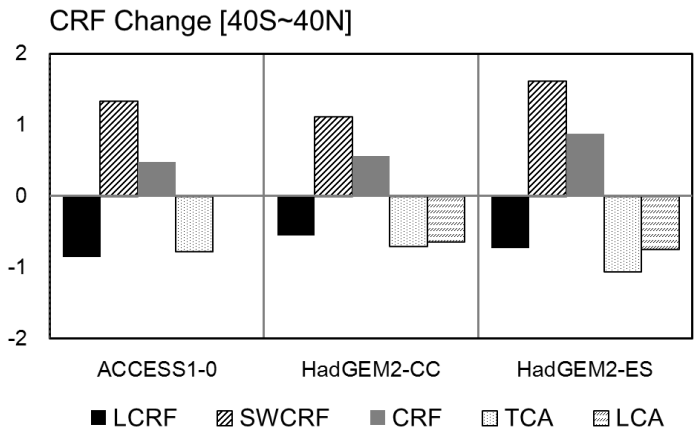

Figure 14 Changes in the cloud radiative forcing in the longwave (LWCRF), and shortwave (SWCRF), net radiative forcing (CRF), total cloud cover (TCA) and low cloud cover (LCA). The actual values are divided by the surface temperature increases, which are different among the models, to give the unit $Wm^{-2}K$-1 for the fluxes, and %K-1 for the cloud cover. Each value is averaged over the ocean across 40S–40N in latitude and 0–360 in longitude Note ACCESS1-0 does not provide the cloud fraction so low cloud cover cannot be obtained.

5. Transient trends

5.1 Cloud cover and CRF

This section discusses transient trends of clouds and their impact on climate, obtained from the B3MME. In Fig. 15, we compare the multi-model averages of the total cloud cover, cloud radiative forcing and global surface temperature using hindcasts/projections for the RCP4.5, beginning in 1901 and ending in 2100. The shading indicates the model uncertainty defined by inter-model difference. The anomalies were obtained against climatology from 1901 to 2005. The B3MME (blue line) shows the decreasing trend of the cloud cover, which is almost the same as that for the low cloud cover but for the rapid decrease in future climate (not shown). The global mean cloud anomaly reaches about -1.1% by 2100, compared against the climatology of 1901–1950. Combined with a strong decreasing trend of the global mean cloud cover from 2000 to 2100, the simulated cloud radiative forcing shows an abrupt increasing trend, corresponding to the reduction of the shortwave cooling

effect by low clouds. We should also note that the trend of global mean temperature is consistent with that of global mean cloud radiative forcing in a future rapid warming period, indicating the role of positive feedback in the climate change.

It is important to note that changes in cloud differ hugely between the northern (NH) and the southern hemispheres (SH) (Fig. 16). The NH cloud cover will be dramatically decreased, reaching -2.0% by the year 2100, while the SH cloud cover will slightly decrease which is not statistically significant. The evident reduction of total cloud cover (mainly by reduction of the low cloud) in the NH may lead to the reduction of the cloud cooling effect, which favors intensification of NH temperature, representing a positive feedback of clouds on the Earth. The difference in cloud change between the NH and the SH will result in a change in the hemispheric thermal contrast: the NH will be warmed much more than the SH, which will increase the thermal contrast and may lead to a change in atmospheric circulation.

In the future climate projection, the MME from 21 models (red line) and the B3MME (blue line) show good agreement in global warming and the reduction of cloud cover in response to greenhouse gas forcing. In modeling the progression toward the future climate, the CMIP5 models are still quite diverse in simulating the cloud change and feedback, even varying in the sign of feedbacks. This seems to be largely due to the misrepresentation of cloud variation in most CMIP5 CGCMs that are not able to reproduce the observed relationship with large-scale environmental changes. In the B3MME, the model ranges in cloud and CRF changes are considerably reduced with increased confidence, indicating the selected models' projection for the cloud variation may be more reliable than other CMIP5 models.

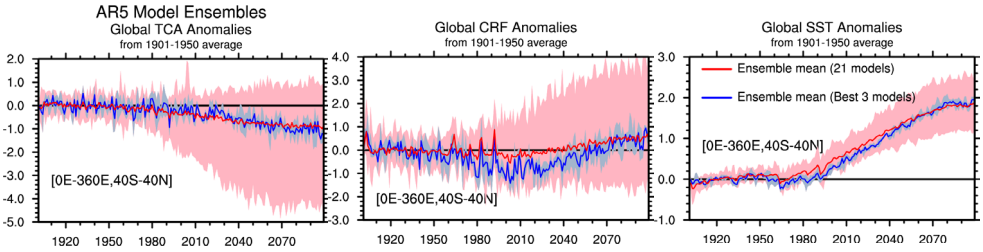

Figure 15 Uncertainties in projected global-mean total cloud amount (TCA), cloud radiative forcing (CRF) and sea surface temperature (SST). Red and blue lines indicate the ensemble means from 21 multi-models (MME) and the selected best 3 models (B3MME) respectively. Shading by pink and sky blue denote the uncertainty range assessed from individual model annual averages used in MME and B3MME, respectively. Annual mean value is averaged over the ocean in the range 40° S-40° N in latitude and 0° E-360° E in longitude. All values are shown as anomalies from the 1901–1950 mean.

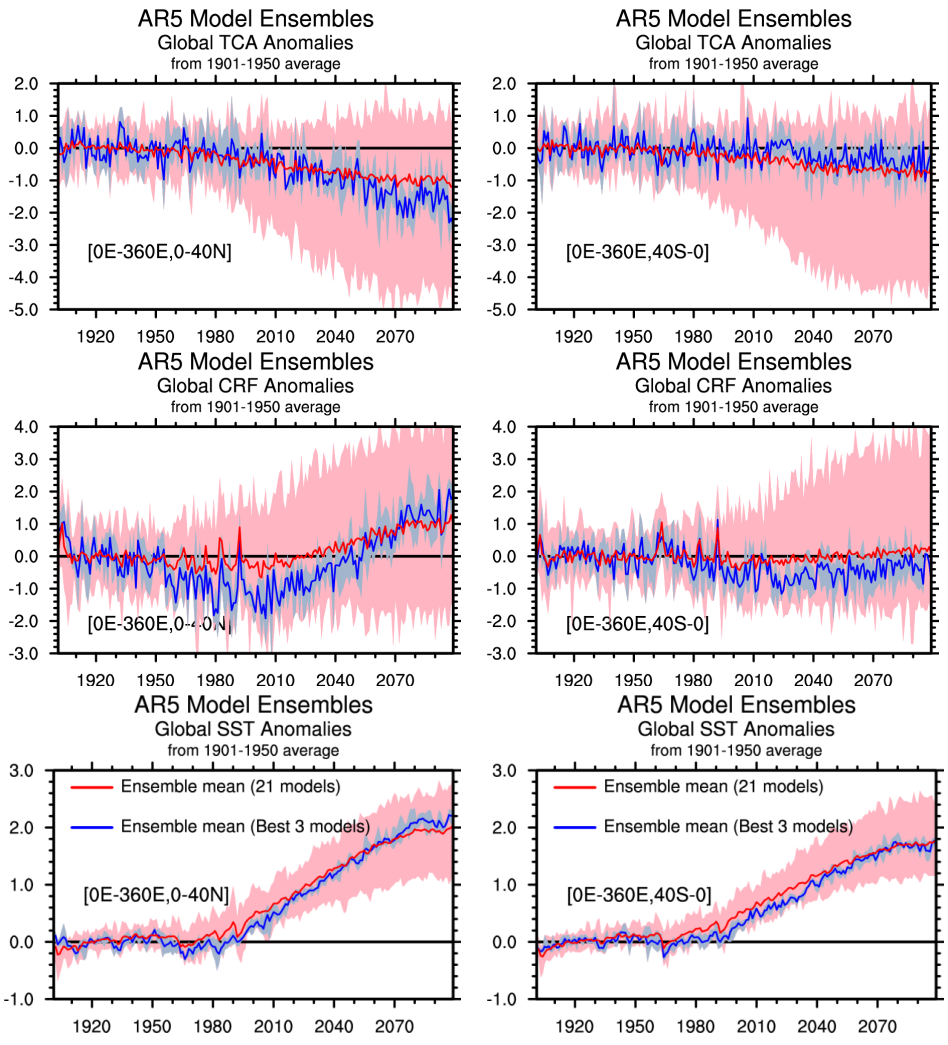

Figure 16 As for Figure 15 but showing (left) the ocean range 0°-40°N in latitude and 0° E-360° E in longitude (northern hemisphere), and (right) the ocean with 40°S-0° in latitude and 0° E-360° E (southern hemisphere).

6. Summary

This study aimed to investigate the degree to which cloud would change and how cloud feedback would operate in a globally warmed climate, using two runs of the 32 CGCMs' simulation and projection in the CMIP5: the historical run under changing solar-volcanic forcing and anthropogenic influences, and the RCP 4.5 run assuming that radiative forcing will stabilize at about 4.5 Wm^{-2} after 2100. By examining the spatial and temporal variation in the observed cloud and its relationship with large-scale environmental conditions, this study suggests a methodology to evaluate the models' performances in simulating the cloud variation, with a primary focus on the low-level clouds. Metrics used for the evaluation include: (1) the annual mean, (2) seasonal variation, and (3) interannual variation in cloud and CRF.

In the examinations of the climatological-mean patterns and their seasonal variation using the ISCCP cloud observations, it was found that the variation in low cloud is closely tied to the variation in low-level tropospheric stability, which is in turn associated with the changes in SST and large-scale subsidence. The low-level cloud shows significant correlation with the lower tropospheric stability (LTS), as well as the sea surface temperature (SST), and sea level pressure (SLP) on an interannual timescale. The correlation coefficients with SST differ in sign, depending on the cloud height: high cloud has a positive correlation with SST while the low cloud has a negative correlation. The spatial pattern of correlation between the total cloud cover and the large-scale variables clearly separates the tropical convective regime dominated by high clouds and the subtropical subsidence regime dominated by low clouds. The mechanisms for the low-level cloud variation were related in such a way that the reduced LTS can be caused by increasing SST, which might cause more vertical motion within and around the cloud deck, leading to the increased entrainment of dry air. This brings about a reduction in low-cloud amount and a tradeoff to high clouds. Higher SLP could also produce more subsidence aloft, increasing LTS independent of SST, and increasing the low-level cloud.

Based on the PCC and NRMSE for the annual mean cloud and seasonal variation, and the cloud-meteorology correlation test for the interannual variation in cloud,

the three best models were selected whose MME has a better skill with much less uncertainty than the 32 model's MME, especially in capturing the low level cloud variations and CRF. The best three models are ACCESS1-0, HadGEM-CC and HadGEM-ES. The selected three best models' MME (B3MME) has a higher skill for the cloud metrics with less uncertainty than other subsets of MMEs over the ocean in the region 40S–40N, 0–360E.

The study further addressed the future changes in cloud and cloud radiative forcing induced by the increase of greenhouse gases, by comparing the climatological cloud simulated by the B3MME during the RCP4.5 run period (2050–2099) with that during the historical run period (1950–1999). In the future climate projection, the selected three models show a good agreement with one another, in the reduction of low-cloud across most of the global oceans in response to greenhouse gas forcing, suggesting a role of positive feedback to climate change by low-level clouds. Spatially, changes in cloud exhibit huge differences between the northern hemisphere (NH) and the southern hemisphere (SH). The difference in cloud change between the NH and the SH will result in a hemispheric thermal contrast change: the NH will be warmed much more than the SH, which increase the thermal contrast and may lead to the change of atmospheric circulation.

In modeling future climate, the CMIP5 models are still quite diverse in simulating the cloud feedback, even varying in the sign of feedbacks. This seems to be largely due to the misrepresentation of low cloud variation in most GCMs that are not able to reproduce the observed relationship of clouds with large-scale environmental conditions. In the B3MME, the model ranges of cloud and CRF changes are considerably reduced with increased confidence, suggesting that the selected models' projections for the cloud variation may be more reliable than other CMIP5 models. These results suggest a more complete method of testing the realism of cloud simulation in current climate models and address how much the model uncertainty can be reduced in climate temperature projections through increasing confidence in cloud feedback.

REFERENCES

Bony, S., *et al.*, 2006: How well do we understand and evaluate climate change feedback processes? J. Clim., 19, 3445-3482.

Bony, S., and J.-L. Dufresne, 2005: Marine boundary-layer clouds at the heart of tropical cloud feedback uncertainties in climate models. Geophys. Res. Lett., 32(20), L20806, doi:10.1029/2005GL023851.

Campbell, G., 2004: View angle dependence of cloudiness and the trend in ISCCP cloudiness, paper presented at 13th Conference on Satellite Meteorology and Oceanography, Am. Meteorol. Soc., Norfolk, Va., 20-23 Sept.

Clement, A.C., R. Burgman, and J.R. Norris, 2009: Observational and model evidence for positive low-level cloud feedback. Science, 325, 460-464. Doi:10.1126/science.1171255.

Evan, A.T., A.K. Heidinger, D.J. Vimont, 2007: Arguments against a physical long-term trend in global ISCCP cloud amounts. Geophys. Res. Lett. 34, L04701, doi:10.1029/2006GL028083.

George, R. C. and R. Wood, 2010: Subseasonal variability of low cloud radiative properties over the southeast Pacific Ocean, Atmos, Chem. Phys., 10, 4047-4063, doi:10.5194/acp-10-4047-2010.

Jacobowitz, H., L.L.Stowe, G. Ohring, A.Heidinger, K. Knapp, and N.R.Nalli, 2003: The Advanced Very High Resolution Radiometer Pathfinder Atmosphere (PATMOS) climate dataset: a resource for climate research. Bull. Amer. Meteor. Soc., 84, 785-793.

Klein, S.A., and D. L. Hartmann, 1993: The seasonal cycle of low stratiform clouds. J. Clim., 6, 1587-1606.

Larson, K., D. L. Hartmann, and S. A. Klein, 1999: The role of clouds, water vapor, circulation, and boundary layer structure in the sensitivity of the tropical climate. J. Clim., 12, 2359–2374.

Meehl, G.A., C. Covey, T. Delworth, M. Latif, B. McAvyaney, J.F.B. Mitchell, R.J. Stouffer, K.E. Taylor, 2007: The WCRP CMIP3 multimodel dataset: a new era in climate change research. Bull. Amer. Met. Soc., 88, 1383-1394.

Norris, J.R., and C. B. Leovy, 1994: Interannual variability in stratiform cloudiness and sea surface temperature. J. Clim., 7, 1915-1925.

Norris, J.R., 2000: What can cloud observations tell us about climate variability? Space Sci. Rev. 94, 375-380.

Norris, J.R., 2005: Trends in upper-level cloud cover and surface divergence over the tropical Indo-Pacific Ocean between 1952-1997. J. Geophys. Res., 110, D21110, doi:10.1029/2005JD006183.

NRC (National Research Council), 2003: Understanding Climate Change Feedbacks. National Academies Press, Washington, DC, 152pp.

Ramaswamy, V. *et al.*, 2001: Radiative Forcing of Climate Change, Chapter 6, pp.349-416.

Randall, D.A., *et al.*, 2006: Cloud feedbacks. In: Frontiers in the Science of Climate Modeling [Kiehl, J.T., and V. Ramanathan (eds.)]. Proceedings of a symposium in honor of Professor Robert D. Cess.

Rossow, W.B., and R.A. Schiffer, 1999: Advances in understanding clouds from ISCCP. Bull. Am. Meteor. Soc., 80, 2261-2287.

Slingo, A. 1990: Sensitivity of the earth's radiation budget to changes in low clouds. Nature, 343-49-51.

Soden, B. J., and I. M. Held, 2006; An assessment of climate feedbacks in coupled ocean-atmosphere

models. J. Clim., 19, 3354-3360.

Stephens, G.L., 2005: Cloud feedbacks in the climate system: a critical review. J. Clim., 18, 237-273.

Stowasser, M., and K. Hamilton, 2006: Relationship between shortwave cloud radiative forcing and local meteorological variables compared in observations and several global climate models. J. Clim., 19, 4344-4359.

Webb, M.J., *et al.*, 2006: On the contribution of local feedback mechanisms to the range of climate sensitivity in two GCM ensembles. Clim. Dyn., 27, 17-38.

Williams, K.D., M.A. Ringer, C.A. Senior. M.J. Webb, B.J. McAvaney, N. Andronova, S.Bony, J.-L. Dufresne, S. Emori, R. Guohmura, T. Knutson, B. Li, K. Lo, I. Musat, J. Wegner, A. Slingo, and J.F.B. Mitchel, 2006: Evaluation of a component of the cloud response to climate change in an intercomparison of climate models. Clim. Dyn., 26, 145-165.

Wood, R., and D.L. Hartmann, 2006: Spatial variability of liquid water path in marine low clouds: The importance of mesoscale cellular convection. J. Clim., 19, 1748-1764.

Wyant, M.C., C.S. Bretherton, H. A. Rand, and D.E. Stevens, 1997: Numerical simulations and a conceptual model of the stratocumulus to trade cumulus transition. J. Atmos. Sci. 54, 169-192.

Wyant, M.C., C.S. Bretherton, J.T. Bacmeister, J.T. Kiehl, I.M. Held, M. Zhao, S.A. Klein, and B.J. Soden, 2006: A comparison of low-latitude cloud properties and their response to climate change in three US AGCMs sorted into regimes using mid-tropospheric vertical velocity. Clim. Dyn., 27, 261-279.

Wylie, D., D.L. Jackson, W. P. Mensel, and J.J. Bates, 2005: Trends in global cloud cover in two decades of HIRS observations. J. Clim.. 18. 3021-3031.

Zhang, M., 2004: Cloud-climate feedback: how much do we know? In: Observation, Theory and Modeling of Atmospheric Variability, World Scientific Series on Meteorology of East Asia, Vol. 3 [Zhu *et al.* (eds)]. World Scientific Publishing Co., Singapore, 632pp.

APCC TECHNICAL REPORT 2012-03

- An Assessment of Reliability in Climate Projections : Cloud Variation
- An Evaluation of the Ability of CMIP5 Multi-Models to Predict Interdiurnal Variability
- Climate Change Projection of South Asian Summer Monsoon
- The Role of the Western Pacific Oscillation Teleconnection Pattern

APEC Climate Center

12, Centum 7-ro, Haeundae-gu, Busan 612-020,
Republic of Korea
Tel: +82-51-745-3900 Fax: +82-51-745-3949
www.apcc21.org

비매품
9 788997 133387
ISBN 978-89-97333-38-7
ISBN 978-89-97333-35-6 (세트)